INDIAN JOURNAL OF SCIENCE AND TECHNOLOGY

RESEARCH ARTICLE

Structural and Electrical Studies of Polycrystalline $Pr_xY_{1-x}FeO_3$ Materials Prepared Through Sol-Gel Route

T Devender Reddy[1], G Padmasree[2]*, P Yadagiri Reddy[1], Ch Gopal Reddy[1]*

1 Department of Physics,, Osmania University, Hyderabad, 500007, India
2 Stanley College of Engineering & Technology for Women, Hyderabad, 500001, India

OPEN ACCESS

Received: 07-08-2024
Accepted: 19-08-2024
Published: 27-08-2024

Citation: Reddy TD, Padmasree G, Reddy PY, Reddy CG (2024) Structural and Electrical Studies of Polycrystalline $Pr_xY_{1-x}FeO_3$ Materials Prepared Through Sol-Gel Route. Indian Journal of Science and Technology 17(34): 3589-3597. https://doi.org/10.17485/IJST/v17i34.2540

* **Corresponding authors**.

gpadmasree@stanley.edu.in

ch_gopalreddy@yahoo.com

Funding: None

Competing Interests: None

Published By Indian Society for Education and Environment (iSee)

ISSN
Print: 0974-6846
Electronic: 0974-5645

Abstract

Objectives: Investigations on structural, morphological and electrical studies of Pr substituted $YFeO_3$ samples synthesized through sol-gel route are presented in this paper. **Methods:** $Pr_xY_{1-x}FeO_3$ (x=0.0, 0.2, 0.4, 0.6, 0.8 and 1.0) samples are synthesized by sol-gel auto combustion method. Structural characterization of the samples is done by using X-ray diffraction (XRD), Field emission scanning electron microscope (FESEM) and Energy dispersive X-ray (EDX) techniques. Electrical properties are studied by J-E and
Ln J-Ln E measurements. **Findings:** Rietveld refined XRD structural analysis shows sharp intense peaks indicating the crystalline nature of the samples and all the samples possess distorted orthorhombic structure with space group *Pbnm*. FESEM analysis shows non-uniform nature of grain size with increasing porosity. EDX data confirms elemental composition, weight and atomic percentage of the prepared samples which further confirms their purity. The leakage current density increases with increase in Pr doping. The slopes of Ln J-Ln E graphs of all the samples are in the range of 1.11 to 1.51 confirming that Ohmic conduction is predominant conduction mechanism. **Novelty**: Investigations on the effect of Pr substitution on electrical properties of single phase $YFeO_3$ samples reveal that the substitution of Pr in $YFeO_3$ decreases the ferroelectric nature of the samples.

Keywords: Sol-gel method; XRD; FESEM; EDX; Electrical Properties

1 Introduction

Multiferroic materials exhibit at least two or more ferroic orders, such as ferroelectricity, ferromagnetism, and ferroelasticity [1,2] in single phase. These multiferroic materials have an intriguing feature called magneto-electric coupling, which combines magnetic and electric orders [3]. Multiferroics are widely used in a wide range of applications, including storage devices, solar energy devices, transducers, sensors, bubble memory devices, permanent magnets, optoelectronics, satellite communication and photoelectron chemical cells [4–6].

Perovskite type orthoferrites exhibit multiferroic properties and possess unique structural and electrical properties. Because of their diverse physical properties, large applications are seen in the present era of technology. Orthoferrites having $RFeO_3$ (where R is rare earth element) general formula is gaining attention of scientific community[7]. At room temperatures, $RFeO_3$ polycrystalline materials have distorted perovskite structure characterized by space group of *Pbnm*. As $YFeO_3$ exhibits multiferroic features of possessing both ferroelectric and weak ferromagnetic nature at ambient temperature, researchers are becoming more interested in it compared to other multiferroic materials. Due to its magneto-optical phenomena, $YFeO_3$ perovskite can be used as memory element in logical devices, optical switches, magnetic field sensors and magnetic and optical current sensors. $YFeO_3$ possesses perovskite structure with *Pbnm* space group[8]. The Y cation is coordinated by 12 oxygen anions, while the Fe cation is surrounded by six oxygen anions. While two adjoining octahedral sites share oxygen, each ferric cation at the octahedral site in $YFeO_3$ is surrounded by six surrounding magnetic ions and organized as FeO_6.

Ferroelectricity is generally not seen in centro symmetric phase groups like *Pnma*/*Pbnm*. But in $YFeO_3$ which belongs to *Pbnm* phase group, ferroelectric ordering is observed even at room temperature[9]. However, there is a meager study on room temperature ferroelectricity exhibited by centro symmetric phase groups like *Pnma*/*Pbnm*. Earlier works on orthoferrites and transition metal oxides have shown that the structural and physical properties can be modified by doping[10]. Zaghrioui et al.[11] and Cheng et al.[12] have observed that doping of transition metals in $YMnO_3$ and $BiFeO_3$ has affected the magnetic properties of the compound. As $YFeO_3$ possesses the same crystallite structure as of these compounds, the physical properties of $YFeO_3$ are also expected to be effectively modified by doping. These modifications in their properties can be used to explore different applications in technical fields. Doping with different elements has been proved to be very effective in improving magnetic and ferroelectric properties in $YFeO_3$. In $BiFeO_3$, doping of Mn enhances the magnetic moments. Bharadwaj et al.[13] studied structural, optical and magnetic properties of Sm^{3+} doped yttrium orthoferrite ($YFeO_3$) and found that lattice parameters increased with Sm^{3+} concentration. Suthar et al.[14] reported structural, electrical, thermal and optical properties of $YFeO_3$, prepared by solid state reaction method. In previous studies most of the researchers used solid state reaction technique which is a very slow and lengthy process requiring high temperatures and with product containing lot of impurities in it. However, in our study an innovative sol-gel method is used requiring less time and temperature compared to solid state method. The end product prepared by this method is obtained in its pure form and size and morphology are easily controlled. Going through the literature, it is understood that not much of study is reported on the preparation of $Pr_xY_{1-x}FeO_3$ materials and no observations of the structural, morphological and electrical properties of these materials are reported. Hence, present research work has been undertaken.

The primary aim of present work is to analyze the effect of Praseodymium (Pr) doping on the electrical properties of $YFeO_3$ samples and an attempt is made to correlate them to the crystallographic changes occurring in the samples with Pr doping. Present work primarily focuses on investigating the changes occurring in the structural, morphological and electrical properties of $Pr_xY_{1-x}FeO_3$ samples due to the Pr content.

2 Methodology

Polycrystalline $Pr_xY_{1-x}FeO_3$ (x=0.0, 0.2, 0.4, 0.6, 0.8 and 1.0) samples are prepared using sol-gel auto-combustion method. Yttrium oxide (Y_2O_3) is weighed in a stoichiometric ratio and dissolved in nitric acid (HNO_3) to form nitrates. Iron (III) nitrate nonahydrate [$Fe(NO_3)_3.9H_2O$] is dissolved in water and its clear solution is obtained. Citric acid is taken in 1:1 ratio with metallic ion and is dissolved in water. Praseodymium oxide (Pr_6O_{11}) is dissolved in nitric acid and is constantly stirred to obtain a clear solution. All the prepared solutions of Y_2O_3, $Fe(NO_3)_3.9H_2O$, citric acid and Pr_6O_{11} are added together and continuously stirred for 30 minutes. The p^H of the solution is adjusted to neutral by adding ammonium hydroxide (NH_4OH) solution drop wise and the neutral solution is heated and stirred continuously for 4 hours. When the volume of the solution is reduced to one-third of its original volume, ethylene glycol is added in a ratio of 1:1.2 to turn the solution into gel. The obtained gel is then heated at 150 °C until it turns into brown fluffy ash. This ash is then finely grinded to get powder and is calcined at 600 °C for 4 hours to remove volatile gases. These samples are then densely pelletized using a pelletizer machine and sintered at 1200 °C for 4 hours in a hot furnace.

The Bruker D8 Advance X-Ray diffractometer with Cu-K_α radiation is used for the XRD measurements, which are used to study the structural characteristics of the materials. Zeiss EVO 18 device is used to obtain the Energy Dispersive X-ray (EDX) spectra of all the samples and EDX images. The micrographs of the samples are recorded using a Field Emission Scanning Electron Microscope (FESEM) device (Carlzeiss Ultra 55 Model of Oxford), which provides information about the grain size and surface morphology of the samples. For studying the ferroelectric properties of the samples at room temperature, Radiant-II, USA made system is used.

3 Results and Discussion

3.1 Structural Analysis

Figure 1 shows Rietveld refined X-ray diffraction (XRD) graphs of praseodymium (Pr) doped yttrium iron oxide ($YFeO_3$) samples. The sharp peaks of the samples with high intensity indicate good crystallization. All these samples have distorted orthorhombic structure having space group *Pbnm* as reported in the literature[15]. For the pure $YFeO_3$ sample (i.e. for x = 0.0), small impurity peak is detected at 27^0 whichis due to residue of Y_2O_3 originated because of incomplete self-combustion taking place during the formation of the final product. For $Pr_xY_{1-x}FeO_3$ (x=0.2, 0.4, 0.6, 0.8 and 1.0) samples no extra peaks are observed in the XRD graphs which confirm that these samples are in pure phase without any detectable impurities. The Rietveld refined parameters such as residual factor (R_p), weighted residual factor (R_{wp}) and goodness of fit (χ^2) are summarized in Table 1. It is found that the values of the goodness of fit of the samples are less than or around 2 showing that the data fitting is good.

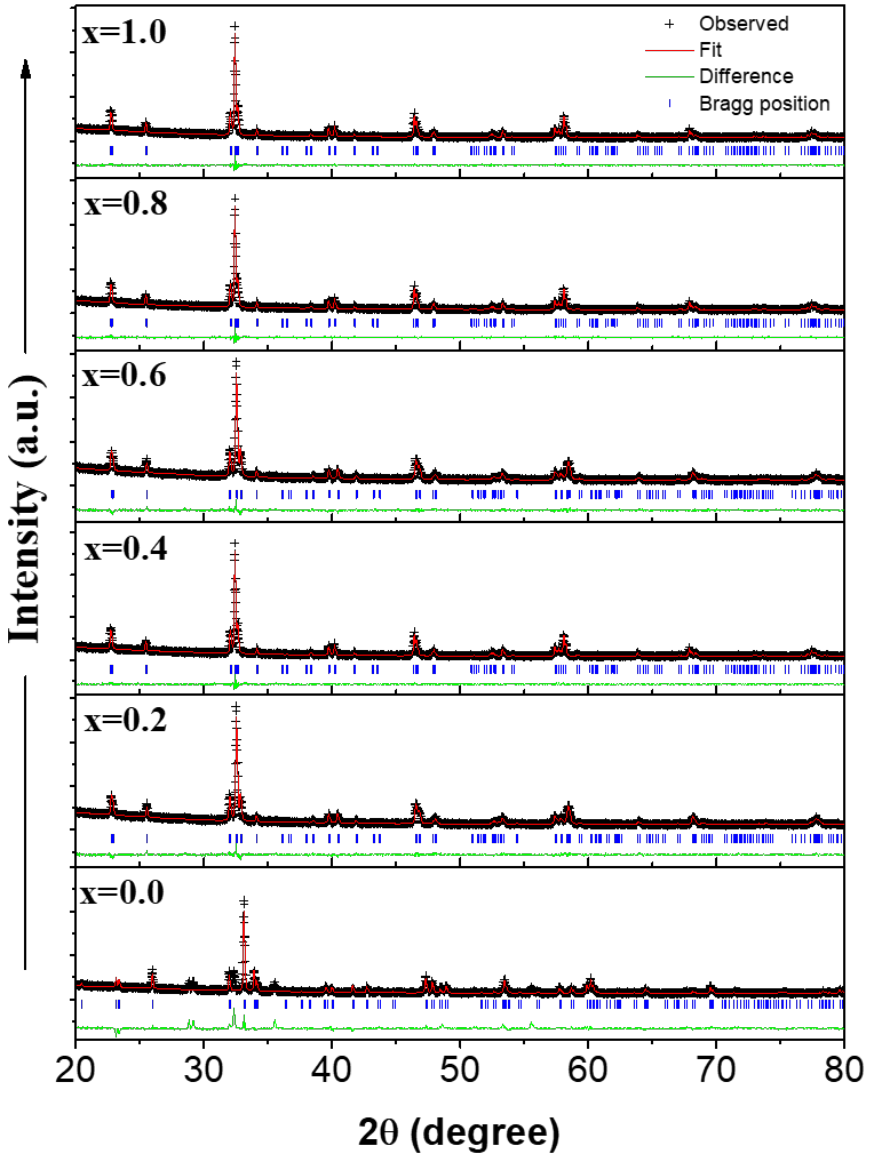

Fig 1. Rietveld refined XRD graphs of $Pr_xY_{1-x}FeO_3$ samples including observed and calculated data along with difference and Bragg reflections

It is observed that lattice parameters and unit cell volume increase with the increase in praseodymium (Pr) concentration (Table 1). This is explained as follows. When large sized praseodymium ion (Pr^{3+}) having atomic number Z=59 and ionic radius = 1.18 A^0 is substituted at the site of yttrium ion Y^{3+} (Z=39, ionic radius = 0.90 A^0), it results in the change of crystal structure. The rotation around the orthorhombic crystallographic axis results in tilted FeO_6 octahedral structure[16]. With increase in praseodymium (Pr) concentration the magnitude of tilting of FeO_6 octahedral structure also increases. When more praseodymium is substituted in place of yttrium, the FeO_6 octahedral structure is tilted much around the crystallographic directions leading to increase of lattice parameters. The increase in lattice parameters indicates that doping of praseodymium in place of yttrium induces distortion in the crystal structure. The increase in the lattice parameters will ultimately lead to an increase in the volume of the unit cell. These changes in unit cell parameters cause corresponding changes in Fe-O bond length and O-Fe-O bond angles that have prominent effects on structural and electrical properties of these materials.

Table 1. Rietveld refined parameters of $Pr_xY_{1-x}FeO_3$ samples

Sample	R_p	R_{wp}	χ^2	a (A^0)	b (A^0)	c (A^0)	Unit cell volume $(A^0)^3$
$YFeO_3$	6.17	9.11	2.07	5.281	5.591	7.603	224.507
$Pr_{0.2}Y_{0.8}FeO_3$	6.48	8.99	1.97	5.321	5.595	7.642	227.502
$Pr_{0.4}Y_{0.6}FeO_3$	5.93	7.63	2.01	5.346	5.605	7.695	230.553
$Pr_{0.6}Y_{0.4}FeO_3$	5.41	8.06	2.54	5.395	5.614	7.721	233.864
$Pr_{0.8}Y_{0.2}FeO_3$	5.85	7.40	1.32	5.447	5.624	7.757	237.611
$PrFeO_3$	5.38	6.82	1.10	5.482	5.637	7.786	240.625

Figure 2 shows the shift of high intensity XRD peak with increase of praseodymium concentration (x) in 2θ range of 31^0 to 34^0. The high intensity peak shifts towards the lower 2θ side with an increase in praseodymium concentration. The shift of high intensity XRD peak towards the lower 2θ side with an increase in praseodymium concentration in 2θ range of 31^0 to 34^0 is explained as follows: When praseodymium ion (Pr^{3+}) having larger ionic radius is substituted at the site of yttrium ion (Y^{3+})having smaller ionic radius, the crystal lattice structure gets distorted and it is evident from Table 1 that unit cell volume increases. Correspondingly, the inter planar spacing (d) also increases as Pr concentration increases. From Braggs law, $2d \sin\theta = n\lambda$, it can be inferred that as nλ is constant, the increase in the value of 'd' results in the decrease of 'θ'. Therefore, as the doping concentration of Pr increases, high intensity peak shift towards the lower side of 2θ.

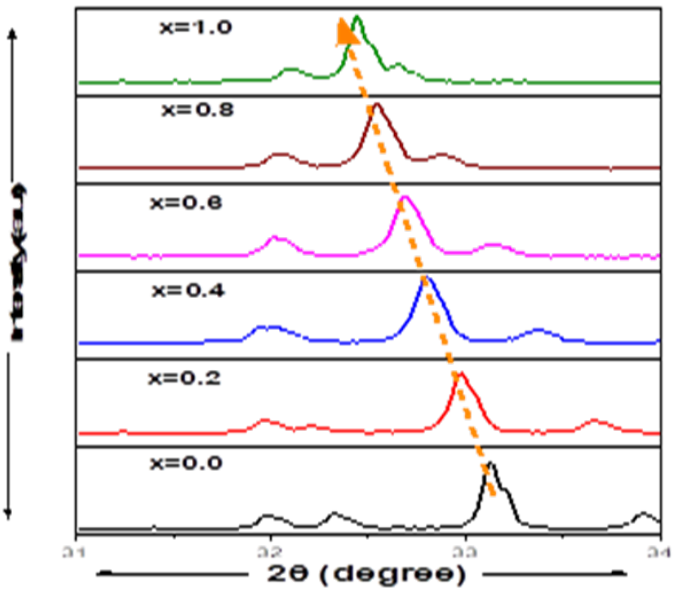

Fig 2. Shifting of high intensity XRD peak with increase of Pr concentration (x)

3.2 Surface Morphology

To understand the micro-structure and arrangement of grains in the samples, Field Emission Scanning Electron Microscope (FESEM) images are obtained. Figure 3 shows FESEM images of $Pr_xY_{1-x}FeO_3$ (x = 0.0, 0.2, 0.4, 0.6, 0.8 and 1.0) samples in the scale of 200 nm. All the samples have non-uniform grain size, and the grains are irregular in shape and size. When praseodymium ion (Pr^{3+}) having larger ionic radius of 1.18 A^0 is substituted at the site of yttrium ion (Y^{3+})having smaller ionic radius of 0.90 A^0, it leads to lattice distortions and potentially create more voids in the crystal structure, which creates porosity in the doped samples. Also as the doping of the praseodymium (Pr) increases the grains are coalescing with each other and as a result porosity increases. This agglomeration of the grains results in an increase in leakage current as the contact between the non-uniform grains leads to charge exchange between the grains called as hetero charging [10]. This change in the grain structure and porosity induces modifications in the electrical properties of the samples.

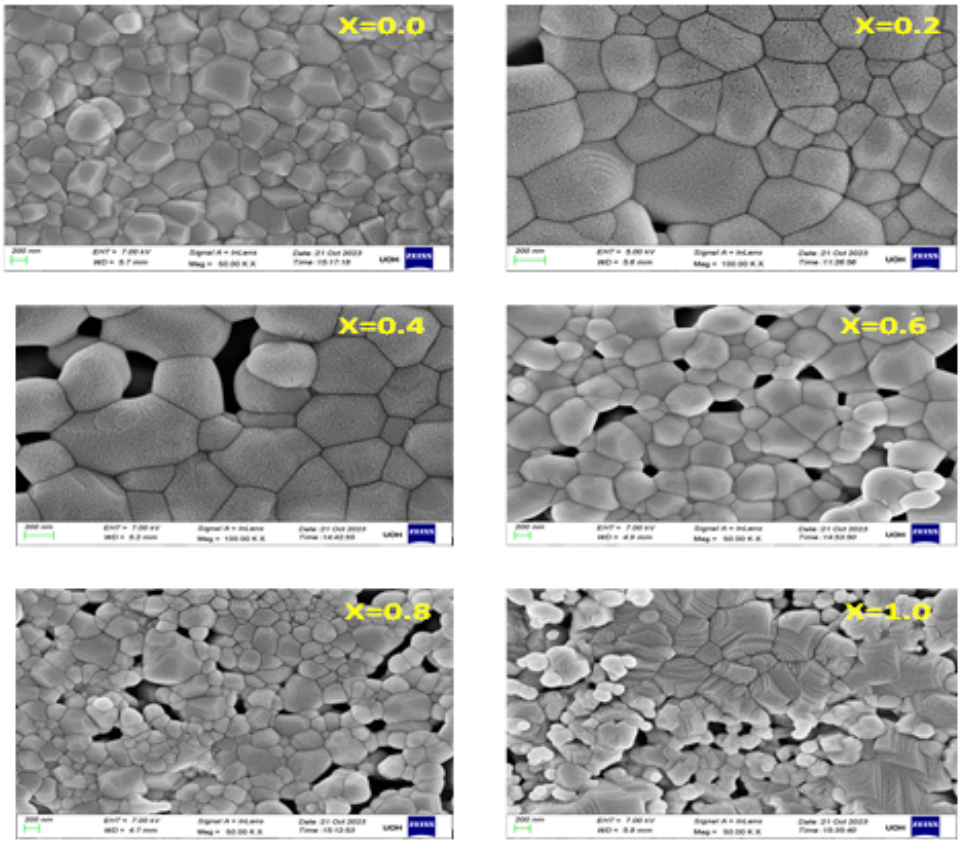

Fig 3. FESEM images of $Pr_xY_{1-x}FeO_3$ samples

3.3 Energy dispersive X-ray (EDX) analysis

Zeiss EVO 18 device is used to obtain the Energy Dispersive X-ray (EDX) spectra of all the samples and EDX images are shown in Figure 4. EDX spectra confirms that the samples are homogeneous and Y, O, Fe, Pr elements are present in the samples, i.e. no detectable impurities are present in the prepared samples which corroborates with the observations of XRD graphs. Table 2 provides estimated weight percentage and atomic percentage of all the chemical elements present in the samples. It is observed that praseodymium weight and atomic percentages gradually increase from x=0.0 to x=1.0 sample and Pr finally occupies the yttrium position.

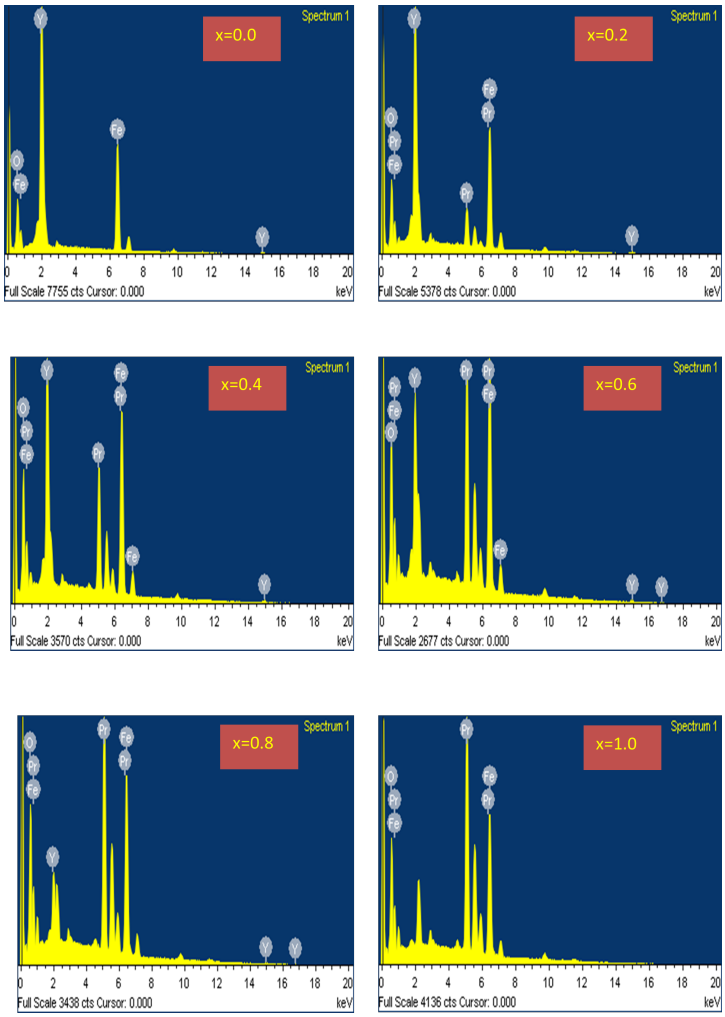

Fig 4. EDX images of $Pr_xY_{1-x}FeO_3$ samples

Table 2. Elemental compositions in weight and atomic percentages in $Pr_xY_{1-x}FeO_3$ samples

Sample composition$Pr_xY_{1-x}FeO_3$	Elements present in the sample	Weight (%)	Atomic (%)
x=0.0	O	22.33	56.22
	Fe	31.98	23.07
	Y	45.69	20.70
x=0.2	O	19.67	54.35
	Fe	28.62	22.66
	Y	36.87	18.33
	Pr	14.84	4.66
x=0.4	O	19.71	56.17
	Fe	26.25	21.43
	Y	25.94	13.30
	Pr	28.11	9.10
x=0.6	O	16.77	52.82
	Fe	25.80	23.28
	Y	16.08	9.11
	Pr	41.36	14.79
x=0.8	O	16.91	54.47

Continued on next page

Table 2 continued

	Fe	24.26	22.39
	Y	7.58	4.39
	Pr	51.25	18.75
	O	14.24	50.63
x=1.0	Fe	24.02	24.46
	Pr	61.73	24.91

3.4 Leakage Current density measurements

For understanding the electrical leaky nature of Pr doped $YFeO_3$ (x = 0.0, 0.2, 0.4, 0.6, 0.8 and 1.0) samples, their leakage current densities (J) are measured with respect to electric field (E). Figure 5 shows the J-E plots which are symmetric about applied electric field. Leakage current density increases continuously from x=0.0 to x=1.0 samples. This increase in leakage current indicates that more substitution of Pr in $YFeO_3$ decreases the ferroelectric nature of the samples. Three main factors affecting the leakage current density in ceramics are concentration of oxygen vacancies, presence of multiple oxidation states of the cation and microstructure of the grains[17]. At higher concentrations, as the larger radius Pr^{3+} ion is substituted in place of smaller Y^{3+} ion, creation of oxygen vacancies increases leading to increase in 'J' value. The other factor is the presence of multiple oxidation states of Fe ions (Fe^{2+} or Fe^{3+} states). From Mossbauer studies the isomer shift value indicates that Fe ion is in its high spin Fe^{3+} state only (not reported in this paper). As discussed in FESEM micrographs, increase in porosity leads to increase in leakage current as fused grain boundaries obstruct the flow of charge carries. Hetero-size charging between the grains occurs due to the non-uniform size which also increases the leakage current. It can be concluded that as leakage current increases significantly the samples are useful for low field applications.

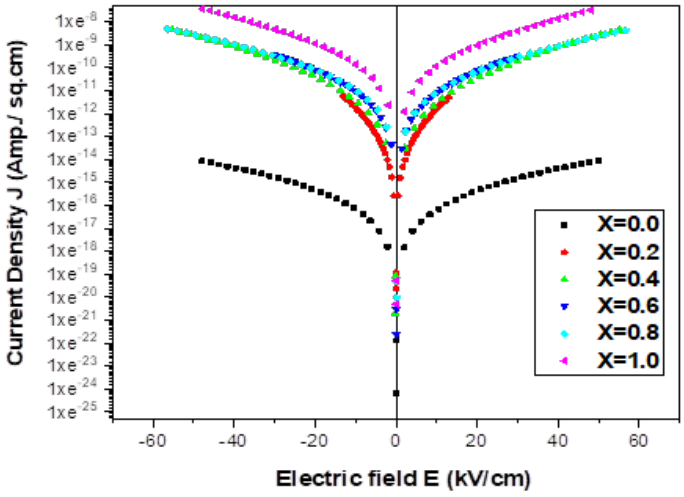

Fig 5. Leakage current density versus Electric field (J-E) plots of $Pr_xY_{1-x}FeO_3$ samples

Ln J versus Ln E graphs give an insight into different conduction mechanisms existing in the samples. Different conduction mechanisms observed in the materials are grain boundary limited conduction, Ohmic conduction, space charge limited conduction, Pool Frenkel emission and Schottky emission, etc. The number of charge carriers in the bulk determines the type of conduction mechanism in those materials. Conduction mechanism is governed by power law equation given by $J \propto E^m$, where 'm' is the slope of straight line in the Ln J-Ln E graph. If m value is < 1, "grain boundary limited conduction" prevails. "Ohmic conduction" dominates if $1 \leq m \leq 2$ and m>2 for "space charge limited conduction"[18]. Figure 6 represents Ln J-Ln E plots of $Pr_xY_{1-x}FeO_3$ samples. For x=0.0, 0.2, 0.4, 0.6, 0.8 and 1.0 samples, the slopes (m) are 1.31, 1.11, 1.29, 1.24, 1.27 and 1.51 respectively which indicates that Ohmic conduction mechanism is predominant in all the samples.

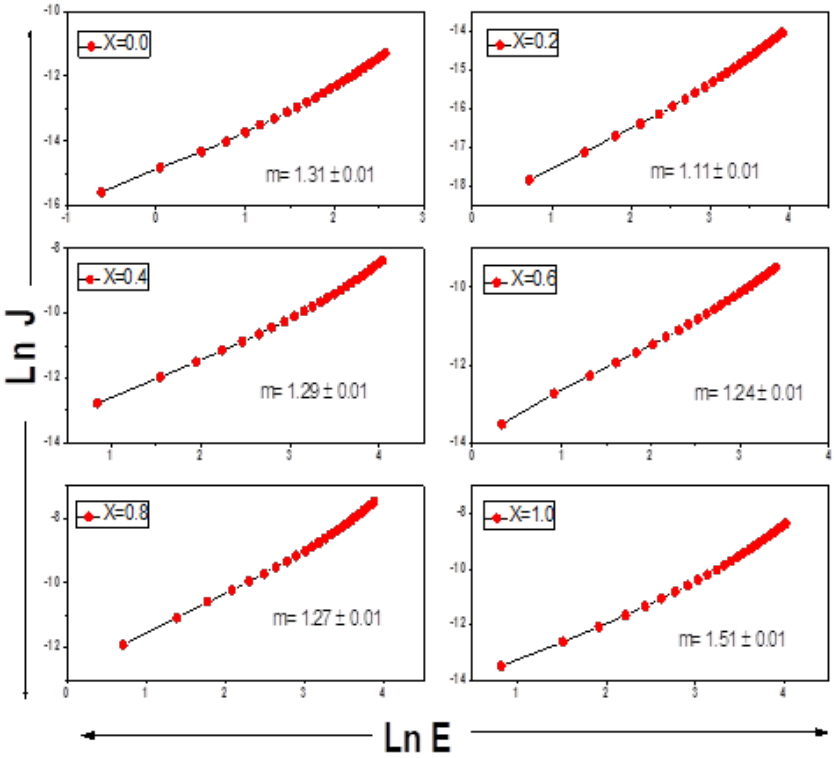

Fig 6. Ln J–Ln E plots of $Pr_xY_{1-x}FeO_3$ samples

4 Conclusions

The polycrystalline $Pr_xY_{1-x}FeO_3$ (x=0.0, 0.2, 0.4, 0.6, 0.8 and 1.0) samples are synthesized using sol-gel auto-combustion method. By using this method pure single-phase compounds are easily synthesized. Rietveld refined XRD structural analysis shows that the samples are crystalline in nature and confirms that the samples possess distorted orthorhombic structure with space group *Pbnm*. It is concluded that doping induces microscopic structural changes in the samples. These changes are attributed to the increase in the values of lattice parameters as doping increases. FESEM analysis shows non-uniform nature of grain size with increasing porosity which leads to increase in leakage current density (J) values. EDX data confirms elemental composition, weight and atomic percentage of the prepared samples which confirms their purity. The leakage current density increases with increase in Pr doping. The slope values of Ln J-Ln E graphs confirm that Ohmic conduction is predominant conduction mechanism in all the samples. From this study it is understood that Pr doped $YFeO_3$ compounds may be used for low field applications in optoelectronic devices. Further studies can aim at finding magneto electric coupling phenomenon in these materials.

Acknowledgements

Authors thank UGC-DAE CSR, Indore, India for sanctioning a project under Collaborative Research Scheme (CRS) with Ref. No: CRS/2021- 22/01/376 for one of the authors (Dr. G. Padmasree) and providing the facilities to carry out the measurements. The authors thank Dr. Vasanth G. Sathe, Centre Director and Dr. V. Raghavender Reddy, Scientist-H and Principal collaborator of the project for guiding us and giving an opportunity to work with UGC-DAE CSR, Indore. Special thanks to Mr. Anil Gome of UGC-DAE CSR, Indore for his support in obtaining XRD, electrical measurements. The authors acknowledge FESEM-EDX facility at Department of Physics, University of Hyderabad for providing FESEM and EDX measurements.

References

1) Ahmed I, Mustafa G, Subhani MU, Hussain G, Ismail GA, Anwar H. A detailed investigation of lanthanum substituted bismuth ferrite for enhanced structural, optical, dielectric, magnetic and ferroelectric properties. *Results in Physics*. 2022;38:105584–105584. Available from: https://doi.org/10.1016/j.rinp.2022.105584.
2) Alanazi IT, Sayed MAE. Structural, optical analysis, stress-strain, and dielectric properties of selenium oxide/LaFeO3/blend nano composites with tunable properties for optoelectronics and micro-supercapacitors. *Journal of Energy Storage*. 2024;95:112652–112652. Available from: https://doi.org/10.1016/j. est.2024.112652.
3) Sadhukhan S, Mahapatra AS, Mitra A, Chakrabarti PK. Multiferroic properties and magnetoelectric coupling observed in nanocrystalline HoFeO3. *Journal of Alloys and Compounds*. 2022;907. Available from: https://doi.org/10.1016/j.jallcom.2022.164443.
4) Maneesha P, Samantaray KS, Baral SC, Brzykcy G, Bhaumik I, Mekki A, et al. Effect of oxygen vacancies and cationic valence state on multiferroicity and magnetodielectric coupling in (1-x) $BaTiO_3$. (x)$LaFeO_3$ solid solution. *Journal of Alloys and Compounds*. 2024;971:172587–172587. Available from: https://doi.org/10.1016/j.jallcom.2023.172587.
5) Sharma S, Kumar M, Laref A, Siqueiros JM, Herrera OR. Recent advances in interfacial engineering and band-gap tuning of perovskite multiferroic heterostructures for high performance photovoltaic applications. *Materials Letters*. 2023;331. Available from: https://doi.org/10.1016/j.matlet.2022. 133490.
6) Zhang Z, Li F, Zheng Y. Highly sensitive resistive humidity sensor based on strontium-doped lanthanum ferrite nanofibers. *Sensors and Actuators A: Physical*. 2023;358:114435–114435. Available from: https://doi.org/10.1016/j.sna.2023.114435.
7) Li CL, Zheng SS, Barasa GO, Zhao YF, Wang L, Wang CL, et al. A comparative study on magnetic behaviors and magnetocaloric effect in heavy rare-earth antiferromagnetic orthoferrites RFeO3 (R = Dy, Ho and Er). *Ceramic International*. 2021;47(24):35160–35169. Available from: https: //doi.org/10.1016/j.ceramint.2021.09.059.
8) Nakhaei M, Khoshnoud DS. Structural, magnetic, and electrical properties of $RFeO_3$ (R=Dy, Ho, Yb & Lu) compounds. *Journal of Materials Science: Materials in Electronics*. 2021;32:14286–14300. Available from: https://doi.org/10.1007/s10854-021-05992-6.
9) Shang M, Zhang C, Zhang T, Yuan L, Ge L. Hongming Yuana, Shouhua Feng. The multiferroic perovskite $YFeO_3$. *Appl Phys Lett*. 2013;102:62903–62903. Available from: https://doi.org/10.1063/1.4791697.
10) Reddy SSK, Raju N, Reddy CG, Reddy PY, Reddy KR, Gupta SM, et al. Study of Mn doped multiferroic $DyFeO_3$ ceramics. *Ceramic International*. 2017;43(8):6148–6155. Available from: https://doi.org/10.1016/j.ceramint.2017.02.010.
11) Zaghrioui M, Greenche JM, Auret-Lambert C, Grevias M. Effect of Fe substitution on multiferroic hexagonal $YMnO_3$. *J Magn & Magn Mater*. 2011;323:509. Available from: http://dx.doi.org/10.1016/j.jmmm.2010.09.055.
12) Cheng ZX, Wang XL, Du Y, Dou SX. A way to enhance the magnetic moment of multiferroic bismuth ferrite. *J Phys D: Appl Phys*. 2010;43:242001–242001. Available from: https://doi.org/10.1088/0022-3727/43/24/242001.
13) Bharadwaj PSJ, Kundu S, Kollipara VS, Varma KBR. Structural, optical and magnetic properties of Sm^{3+} doped yttrium orthoferrite ($YFeO_3$) obtained by sol–gel synthesis route. *Journal of Physics: Condensed Matter*. 2019;32(23). Available from: http://doi.org/10.1088/1361-648X/ab4845.
14) Suthar L, Bhadala F, Roy M. Structural, electrical, thermal and optical properties of $YFeO_3$, prepared by SSR and Sol-Gel route: a comparative study. *Applied Physics A*. 2019;125:452–452. Available from: https://doi.org/10.1007/s00339-019-2743-1.
15) Nagendar V, Srikanth B, Reddy SSK, Raju N, Reddy MS, Reddy CG, et al. Investigation on structural, electrical and magnetic properties of $ErFeO_3$: Sintered at different temperature. *Physica B: Condensed Matter*. 2024;680:415819–415819. Available from: https://doi.org/10.1016/j.physb.2024.415819.
16) Sreedhar Y, Srikanth B, Raju N, Reddy MS, Reddy CG, Reddy PY. Investigation on structural, electrical and magnetic properties: $Dy_{0.4}Sm_{0.6}FeO_3$ orthoferrite with Mn doping at Fe site. *Solid State Communications*. 2024;390:115608–115608. Available from: https://doi.org/10.1016/j.ssc.2024.115608.
17) Kothari D, Reddy VR, Gupta A, Meneghini C, Aquilanti G. Eu doping in multiferroic $BiFeO_3$ ceramics studied by Mossbauer and EXAFS spectroscopy. *Journal of Physics: Condensed Matter*. 2010;22:356001–356001. Available from: https://doi.org/10.1088/0953-8984/22/35/356001.
18) Sundarayya Y, Mandal P, Sundaresan A, Rao C. Mössbauer spectroscopic study of spin reorientation in Mn-substituted yttrium orthoferrite. *Journal of Physics: Condensed Matter*. 2011;23:436001–436001. Available from: https://doi.org/10.1088/0953-8984/23/43/436001.